Torsional fretting and torsional sliding wear behaviors of CuNiAl against 42CrMo4 under dry condition

Po Zhanga, Wenlong Lua, , , Xiaojun Liua, Wenzheng Zhaia, Mingzhuo Zhoua, Wenhan Zengb

a The State Key Laboratory of Digital Manufacturing Equipment and Technology, School of Mechanical Science and Engineering, Huazhong University of Science and Technology, Wuhan 430074, PR China

b EPSRC Centre for Innovative Manufacturing in Advanced Metrology, University of Huddersfield, Huddersfield, HD1 3DH, UK

Abstract

Many wear failures are caused by a combination of fretting wear and sliding wear. In this study, the torsional fretting and torsional sliding wear properties of CuNiAl against 42CrMo4 were comparatively investigated under dry condition using a flat on flat contact tester. Experimental results showed that the sliding friction coefficients declined more dramatically than the fretting friction coefficients when the normal load increased. The fretting wear rate was lower than the sliding wear rate, which was partly due to the solid lubrication effect of the wear debris and strain hardening of the worn surfaces. The dominant wear mechanisms for the fretting tests were oxidation, cracks and delamination, while for the sliding tests were abrasion combined with plastic deformation.

Keywords

Torsional fretting; Torsional sliding; Friction; Wear mechanism

1. Introduction

Torsional wear can be defined as wear under rotational motion of a pair under a normal load. It is widely occurred in the human hip joint, knee joint, slewing ring bearing used in engineering machine, center plate of a bogie, and other reciprocating rotation parts of conveyances [1] ; [2]. Depending on whether the motion amplitude is in micrometer or millimeter scale, it can be classified into torsional fretting wear and torsional sliding wear.

In many engineering applications, the wear failures are caused not just by torsional fretting or torsional sliding but by a combination of them. For example, Fig. 1 shows the cross-section of a controllable pitch propeller (CPP), in which the blade carrier, the blade foot together with the hub form a blade bearing. Godjevac et al. [3] ; [4] reveal that both torsional fretting and torsional sliding wear can happen on the inner radial part of the blade bearing. The fretting wear happens when the pitch is fixed, but due to the fluctuation of wake flow field and rotation of the CPP a maximum 500 μm fretting motion can happen

within the clearances of the bearings. The sliding wear happens when the pitch is adjusted under the push of a hydraulic system. Similarly, in the artificial hip joints and the bogie in a railway carriage, etc., the wear failures are also caused by a combination of torsional fretting and torsional sliding wear [5]; [6] ; [7].

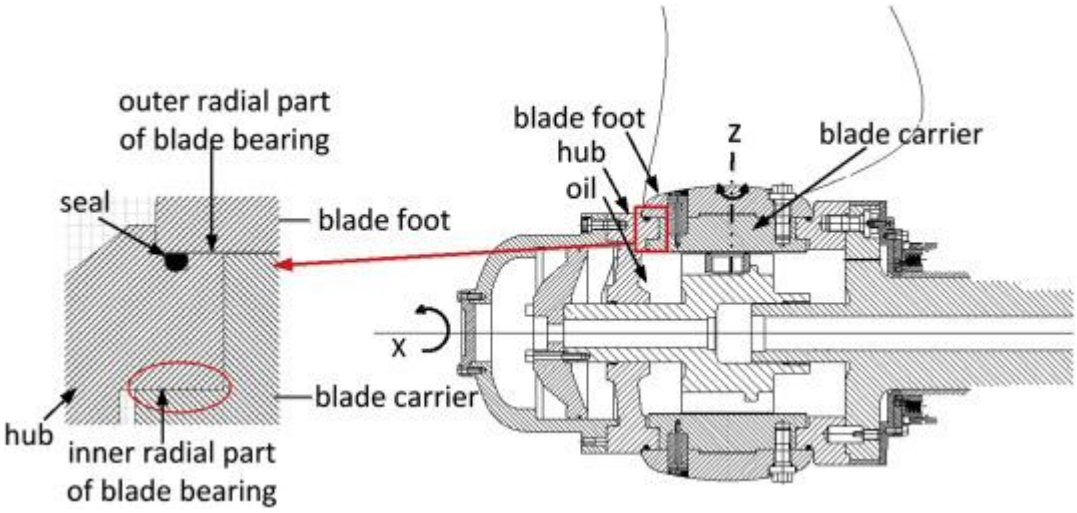

Fig. 1. Assembly of a controllable pitch propeller.

Investigations on torsional fretting and torsional sliding have been reported by many researchers. Quan H et al. [8] evaluated the torsional fretting wear proprieties of three porous bio-coatings modified with anodic oxidation, acid–base treatment, and alkali–heat treatment. Zhang X et al. [9] proposed an efficient numerical model for predicting the torsional fretting wear, which considers the evolution of surface profile variables with the number of fretting cycles. Xu Z B et al. [10] studied the effects of torque and contact pressure on torsional fretting behavior of 316 L austenitic stainless steel in a cylinder-on-cylinder contact configuration. Wang S et al. [11] ; [12] studied the torsional wear behavior of monomer cast nylon (MC nylon) composites reinforced with glass fiber with a self-made torsional friction tester. Chen K et al. [13] investigated the torsional friction contact state and the transformation mechanism of PVA/HA composite hydrogel against CoCrMo femoral head, besides, the effect of load as well as torsional angle on torsional friction behavior was also studied.

However, the above literature review indicates that the torsional fretting and torsional sliding are generally investigated separately rather than comparatively. Besides, the studies are usually carried out under ball on flat contact and rather than under flat on flat contact. The torsional test contact configurations can be basically divided into ball on flat contact, ball on concave contact and flat on flat contact, as shown in Fig. 2. The contact configuration has a great influence on the wear behavior, as the contact stress, contact stiffness, debris behavior are distinctly different under various contact configurations [14]. To better understand the wear mechanisms of the blade bearing, etc., it is necessary to study the torsional fretting and torsional sliding comparatively, and under flat on flat contact rather than commonly used ball on flat contact.

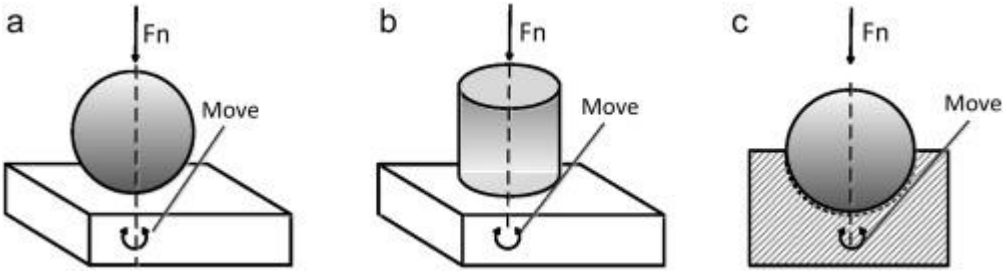

Fig. 2. Torsional fretting wear under different contact configurations: (a) Ball on flat contact; (b) Flat on flat contact; (c) Ball on concave contact.

In this study, the inner radial part of the blade bearing was taken as the research object. The torsional fretting and torsional sliding wear behaviors were comparatively investigated. The tests were carried under dry condition and with a flat on flat contact test rig. Friction behaviors and wear mechanisms were discussed in detail. This investigation can provide some valuable information to understand the wear mechanisms of the blade bearing, and deepen our insight into the torsional wear.

2. Experimental details

2.1. Materials

In the blade bearing, CuNiAl and 42CrMo4 are the common materials used for the hub and blade carrier respectively [3] ; [4]. In this study, CuNiAl was chosen as the material for the lower specimens, and 42CrMo4 was chosen as the material for the upper specimens. Chemical composition of the tested materials are listed in Table 1 ; Table 2. Their physical and mechanical properties are shown in Table 3.

Table 1.
Composition of CuNiAl (wt %).

Al	Si	Mn	Fe	Ni	Cu	Zn	Sn	Pb
9.0–9.5	≤0.1	0.8–1.3	4.5–5.1	4.2–4.8	78.5–80.5	1.5–3.5	≤0.1	≤0.03

Table 2.
Composition of 42CrMo4 (wt %).

C	Si	Mn	P	S	Cr	Mo
0.38–0.45	≤0.40	0.60–0.90	0.035	≤0.035	0.90–1.20	0.15–0.30

Table 3.
Mechanical properties for the friction pair.

Material	Yield strength σ_s (MPa)	Tensile strengthσ_b (MPa)	Elasticity modulus E (MPa)	Poisson's ratio u	Hardness(HB)
CuNiAl	250	650	121,000	0.33	127
42CrMo4	550	800	212,000	0.3	220

2.2. Torsional fretting and torsional sliding tests

The fretting and sliding tests were evaluated on a flat on flat contact torsional wear test rig, which has been described in detail in previous research papers [15] ; [16]. Basically, a closed-loop control step motor (resolution of rotational angle, 0.018°) was used to drive the relative movement between the upper and lower specimens. To ensure that the contact remains flat and the normal load is evenly distributed, the upper holder was designed to be self-aligned, similar with what B.D. Leonard did [17]. By varying the torsional angle of the step motor, both torsional fretting and torsional sliding tests could be carried out on it. A torque sensor (testing range: -2～2Nm, measurement error: less than 0.01Nm) was used to measure the friction torque. Contact between the specimens was designed into a partial ring rather than a full ring, as shown in Fig. 3. The purpose was to reduce the contact area and increase the wear depth so the wear volume could be measured more accurately.

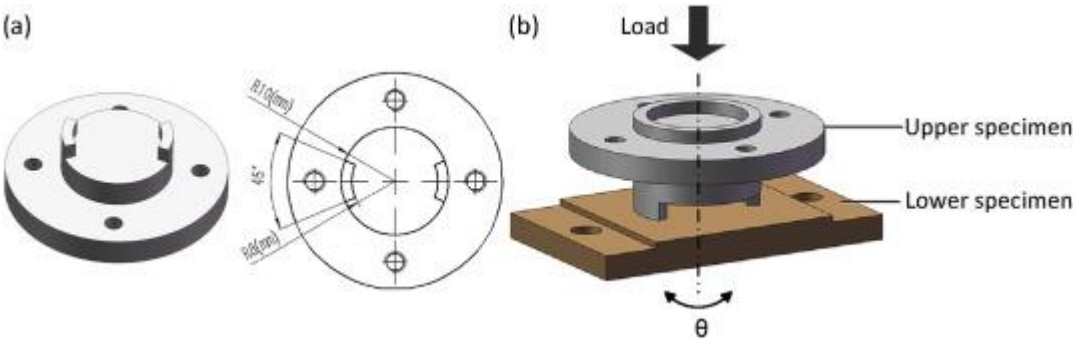

Fig. 3. Schematic diagram of the torsional wear tester: (a) Upper specimen; (b) Contact between the upper and lower specimens.

The angular displacement amplitudes for the fretting and sliding tests were set at 1.5° and 22.5°, respectively, and the corresponding linear displacement amplitudes were 261 μm and 3.925 mm. The number of cycles for per fretting test was set at 60000 and for per sliding test was set at 4000. The total relative angular displacement during each fretting and sliding test was the same of 360000°. The normal loads were selected according to the practical operating condition of the blade bearing and they were set at 43N, 86N and 106N [18]. Sliding speed has been proved to be influential in the sliding wear behavior [19], but its influence on the torsional fretting is unclear. So in this paper, the influence of angular speeds on the torsional fretting and torsional sliding were also investigated. The fretting frequencies were selected within the setting range (1Hz–3Hz) of the test rig. Besides, the test duration and data size were also considered, as under the given number of cycles (60000) smaller fretting frequency means longer test duration and larger data to deal with. In this study, the fretting frequencies were set at 2Hz, 2.5Hz and 3Hz, and the corresponding angular speeds were 12°/s, 15°/s and 18°/s considering the angular displacement amplitude of 1.5°. The angular speeds for the torsional sliding tests were set the same of 12°/s, 15°/s and 18°/s.

2.3. Methods of analysis

During the tests, the variations of friction torque versus torsional angular displacement amplitude were recorded as a function of number of cycles (T-θ-N curves), from which much frictional information could be extracted. Macro wear trace morphologies and wear volumes were obtained by a 3D optical microscope (DSX 510). Micro and cross-sectional morphologies of the wear traces were observed by a field emission scanning electron microscope (FESEM, Helios G3 CX). The Vickers hardness (Hv) of the fretting and sliding wear traces were measured using a Vickers hardness instrument (THVS-1MDX-AXY, load: 200 g, dwell time: 10 s). The chemical compositions of the wear debris were determined by XRF (EAGLE III).

3. Results and discussion

3.1. Friction analysis

In torsional fretting studies, the friction torque versus angular displacement amplitude curves (T-θ curves) are very important as firstly they can reflect the fretting running state, namely partial slip, mixed slip or gross slip. Secondly, by calculating the amplitude of each T-θ curve, which represents the friction torque of a fretting cycle, the friction torque for the whole fretting process can be depicted [15].

Fig. 4 shows the evolution of the typical T-θ curves as a function of number of cycles under different normal loads. It can be seen that all the T-θ curves appeared in the shape of quasi-parallelogram, indicating that the tests were running under gross slip state. The gross slip generally resulted in large amounts of material removal and debris formation. From the amplitude of the T-θ curves it can be seen that in the fretting tests, the friction torque present increasing tendency with the increase of the normal loads; while in sliding tests, at the beginning of the tests, the higher normal load also lead to the higher friction torque, while after a few cycles, the friction torque at 106N turned to be higher than that at 86N. The reason behind this will be discussed later.

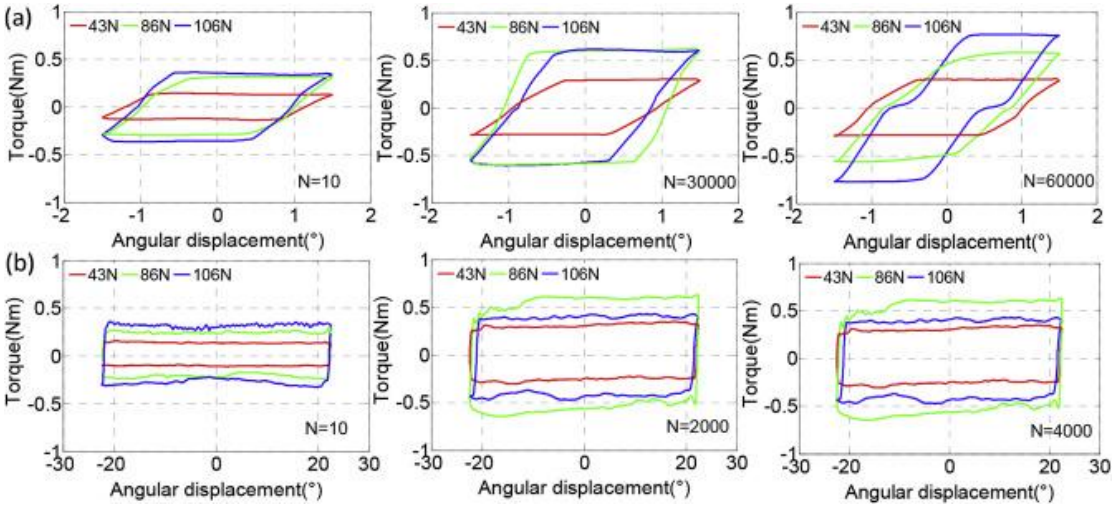

Fig. 4. Typical T-θ curves as a function of number of cycles: (a) Fretting tests (b) Sliding tests (θ = 12°/s).

The evolution of fretting and sliding friction torques as a function of angular displacement to 3.6 × 105(°) is shown in Fig. 5. They mainly exhibit three stages (initial stage, quickly ascending stage and relatively steady stage).

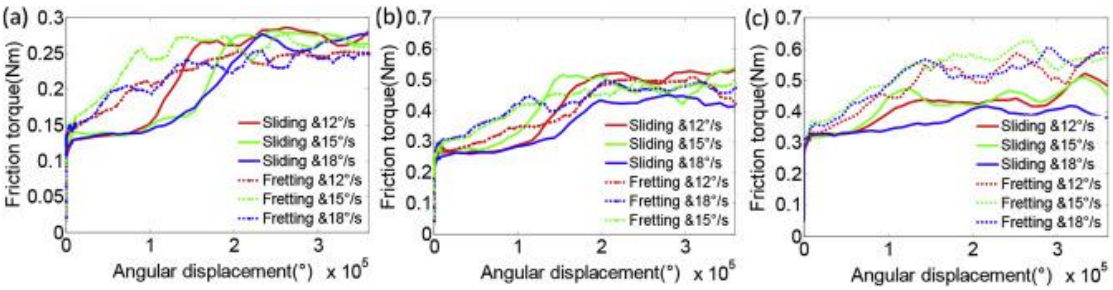

Fig. 5. Evolution of the fretting and sliding friction torque curves: (a) 43N; (b) 86N; (c) 106N.

At the initial stage, both the fretting and sliding friction torques were low due to the presence of a foreign material layer. This layer in general comprised of (i) moisture, (ii) oxide of metals, (iii) deposited lubricating material, etc. They separated the two material surfaces and there was little or no true metallic contact and also the oxide film had a low shear strength [19]. It can also be seen that the initial fretting friction torques were higher than the initial sliding friction torques, which was possibly affected by the real contact area. Before the wear process, the real contact area between the upper and lower specimens was small due to the initial surface roughness and surface shape error. However, the degradation of the initial surface was quicker under fretting condition due to the high frequency and small amplitude. Hence the real contact area and the value of the tangential force due to local plastic deformation were bigger [20] ; [21], leading to the higher initial fretting friction torques.

During the ascending stage, the foreign material layer broke up and clean surfaces came into contact which increased the bonding force. Increase of surface temperature, viscous damping of the friction surface, increased adhesion due to micro-welding or deformation or hardening of the material might had some role on this increment of friction torque as well [19].

After a certain duration of rubbing, many parameters such as the roughness reached a certain steady state value, so the friction torques also ran into a relatively steady state. At the steady stage, the fretting friction torques were slightly lower than the sliding friction torques at 43N, but with the increase of normal loads, the fretting friction torques gradually changed to be higher than the sliding friction torques.

The steady stage friction coefficients of the fretting and sliding tests can be expressed by Refs. [22] ; [23]:

$$\mu = \frac{T}{r \cdot P} \tag{1}$$

where μ refers to the friction coefficient; T is the friction torque; r is the average contact radius and keeps a constant; P is the applied load.

The friction coefficients have been calculated and presented in Fig. 6, which indicates that when the normal load increased, both the fretting and sliding friction coefficients decreased. The reason behind the phenomenon will be explained in the following. The contact radius r keeps a constant during the test, so when the normal load increased, the variation of μ was decided by the increase level of T and P, as shown in Eq. (1). According to the previous studies [24] ; [25], under higher normal load, the rubbing surfaces had a higher temperature, which promoted the formation of oxide scales such as CuO or Al2O3 on the specimen surface. The brittle and fragile oxide scales could contribute to reduce the friction, leading to lower increasing level of the friction torque T than that of the normal load P, which can be seen in Fig. 5. Take Fig. 5(a) and (b) as an example, from P = 43N–86N, the applied normal load increased 2 times, but the steady friction torques increased less than 2 times, so when the normal load increased, the friction torques increased less times than the normal load, thus the friction coefficient decreased when the normal load increased.

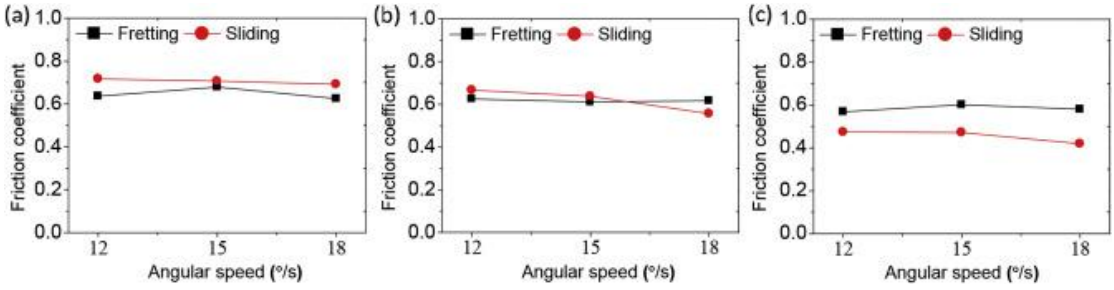

Fig. 6. Fretting and sliding friction coefficient: (a) 43N; (b) 86N; (c) 106N.

It can also be observed from Fig. 6 that at 43N the fretting friction coefficients were about 10% lower than the sliding values, but when the normal load increased to 106N the fretting coefficients turned to be about 30% higher than the sliding values. This was mainly due to the different influence of normal load on the fretting and sliding friction coefficients. As can be seen from Fig. 6 that from 43N to 106N, the fretting friction coefficients decreased about 10%, while the sliding friction coefficients decreased about 36%. So we can know from the phenomenon that, compared with the fretting friction coefficient, the sliding friction coefficients was more sensitive to the increase of normal load.

With respect to the influence of angular speed, it can be seen from Fig. 6 that the increase of sliding speed lead to the decrease of sliding friction coefficients, while it had no regular effect on the fretting friction coefficient. The phenomenon is in consistence with the previous findings. Under sliding condition, when velocity increases, momentum transfer in the normal direction increases producing an upward force on the upper surface. This results in an increased separation between the two surfaces which will decrease the real area of contact. Contributing to the increased separation is the fact that at higher speeds, the time during which opposite asperities compress each other is reduced increasing the level on which the top surfaces move [19] ; [26]. Besides, high sliding speeds can result in high interface (flash) temperatures that can significantly reduce the strength of most materials [27]. Under fretting condition, the increase in speed is in fact the influence of frequency

under the fixed angular amplitude. The effect of frequency on the fretting friction coefficient is complicated. Zhang et al. [28] indicates that under dry condition, the friction coefficient of nanocrystalline surface layer of copper increase with an increasing frequency; while under oil lubrication it firstly increase with an increasing fretting frequency until a maximum value and thereafter descends [29]; Huang et al. [30] found that no detective effect of frequency on the coefficient of friction occurred during the reciprocating fretting tests; Ding et al. [31] observed that the friction coefficient of micro-arc oxidation (MAO) coating of Al2O3 decreases with an increase of the frequency.

3.2. Wear rate

Under fretting tests, the energy dissipated by friction is now widely used to characterize the material response, and usually a linear relationship between accumulated dissipated energy and wear volume can be observed:

$$V=\alpha\cdot\sum Ed+\beta \quad (2)$$

where V is the wear volume, Ed is the accumulated dissipated energy, α is the energetic wear coefficient, and β is the energy used to activate Tribologically Transformed Structure (TTS) and create wear debris during the first phase of test [32].

So the energetic wear coefficient (α) can be calculated:

$$\alpha = \Delta V/\Delta\sum Ed \quad (3)$$

Not only in fretting tests, the energetic approach has also been proved to be effective in evaluating the wear rate of sliding tests [33] ; [34]. So in this study, to facilitate the comparison, both the fretting and sliding wear rates were characterized by the energetic wear coefficient.

The wear volumes were firstly acquired. According to the Archards' model, there is a negative correlation between wear rate and hardness of the material [35]. As the upper specimen (42CrMo4, HB: 220) was harder than the lower specimen (CuNiAl, HB: 127), so after the tests, mainly the wear of the lower specimen was considered. Before acquiring the wear volume, the worn specimens were firstly ultrasonically cleaned in dilute sulfuric acid and ethyl alcohol to remove the wear debris. Then 3D morphologies of the worn scars were obtained with a 3D optical microscope. Finally the wear volumes were obtained by calculating the valley volume below the reference plane [36].

The dissipated energy of each individual fretting cycle (Efi) can be calculated by integrating the surface area of the T-θ curve, as shown in Fig. 7; accumulated dissipated energy (Edf) can be estimated by adding energy dissipated in all cycles. The accumulated dissipated energy of a fretting test can be mathematically defined as [37]:

$$E_{df}=\sum_{i=1}^{60000}E_{fi} \quad (4)$$

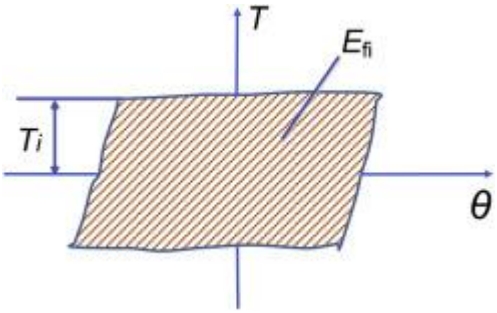

Fig. 7. Friction torque versus angular displacement amplitude curve (T-θ curve).

The dissipated energy of each individual sliding cycle (Esi) and the accumulated dissipated energy of a sliding test (Eds) can be calculated in the similar method, and Eds can be defined as:

$$E_{ds} = \sum_{i=1}^{4000} E_{si} \tag{5}$$

The measured wear volumes and calculated accumulated dissipated energy are presented in Table 4 and Table 5, respectively. The average values under the same normal load but different angular speeds are also presented in the tables.

Table 4.
Fretting and sliding wear volumes.

Load(N)	Fretting wear volumes (× 10^5μm^3)				Sliding wear volumes (× 105μm3)			
	12°/s	15°/s	18°/s	Average	12°/s	15°/s	18°/s	Average
43	670	590	490	**580**	3070	2370	2600	**2680**
86	1460	1900	1590	**1650**	8860	9360	11660	**9660**
106	2450	2990	3450	**2960**	19870	17500	15630	**17660**

Table 5.
Fretting and sliding accumulated dissipated energy.

Load(N)	Fretting accumulated dissipated energy (J)				Sliding accumulated dissipated energy (J)			
	12°/s	15°/s	18°/s	Average	12°/s	15°/s	18°/s	Average
43	1344	1500	1332	**1392**	1297	1378	1333	**1336**
86	2489	2677	2659	**2608**	2698	2697	2307	**2567**
106	2907	3295	3176	**3126**	2876	2715	2350	**2647**

Table 4 indicates that under the same angular speeds, the wear volume increased with the increase of normal load, which was due to the fact as the normal load increases, the frictional heat generates at the contact surface increases and hence strength of materials decreases [19] ; [38]. The influence of angular speed on the wear volume was complicated. When the angular speed increased, the wear volume presented increasing or decreasing or first increasing and then decreasing tendency at different normal load.

From Table 5 it can be seen that under the same angular speed, the accumulated dissipated energy increased with the increase of normal load. Under fretting condition, increase of angular speeds lead to the first increasing and then decreasing tendency of the accumulated dissipated energy. While under sliding tests, the angular speed presented no regular influence on the accumulated dissipated energy.

In Fig. 8, the averaged wear volumes versus the averaged accumulated dissipated energy under different normal loads of the fretting and sliding tests have been plotted. It can be observed that in fretting tests, the wear volumes increased almost linearly with the increase of accumulated dissipated energy. So for the fretting tests, the energetic wear coefficient was:

$$\alpha\ F=1.23\times105\mu m3/J \qquad (6)$$

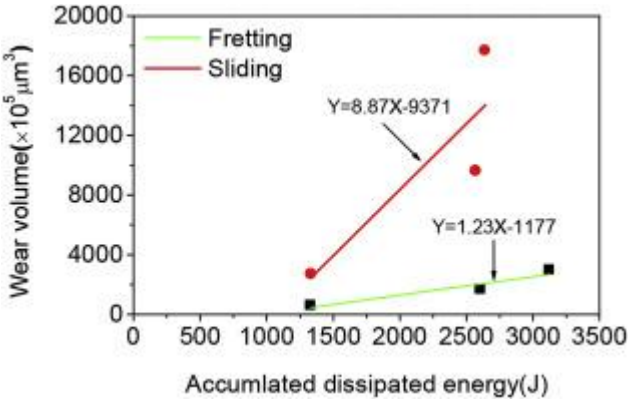

Fig. 8. Wear volume versus accumulated dissipated energy of fretting and sliding tests.

Comparatively, in the sliding tests, the test data scatter a litter far from the fitting straight line, in other words, the liner relationship between the wear volume and the accumulated dissipated energy was not that good. But the slope of the fitting line can still have a general reflection of the energetic wear coefficient, which was:

$$\alpha\ S=8.87\times105\mu m3/J \qquad (7)$$

So it can be seen that the sliding wear rate was times higher than the fretting wear rate. The main reasons for this were the difference in strain hardening of the wear track and debris lubrication effect under the fretting and sliding tests, which will be discussed in the next section.

3.3. Wear scar observation

Typical optical and the corresponding 3D morphologies of the wear traces are shown in Fig. 9. It can be seen that the fretting wear trace presents black color (Fig. 9(a)), indicating that serious oxidation wear occurred. Under dry fretting condition, much frictional heat was generated. The worn surface was burned by the high temperature and then oxidized by reacting with the oxygen from the air. The sliding wear trace is mainly characterized by serious plow wear evidenced by a lot of grooves paralleling the sliding direction (Fig. 9(b)). From the 3D morphologies in Fig. 9(c) and (d) it can be seen that the surface roughness and isotropy of the fretting wear trace are higher than the sliding wear trace. From the 3D and 2D cross-sectional fretting and sliding profiles in Fig. 10 it can also be seen that the fretting wear trace is rougher than the sliding wear trace, which is possibly one of the reasons why the fretting coefficient is higher than the sliding friction coefficient at 106N. The 2D cross-sectional profile presents that the fretting wear depth is shallower than the sliding wear trace, which is in accordance with the results that the wear volumes of the sliding tests are much higher than that of the fretting tests.

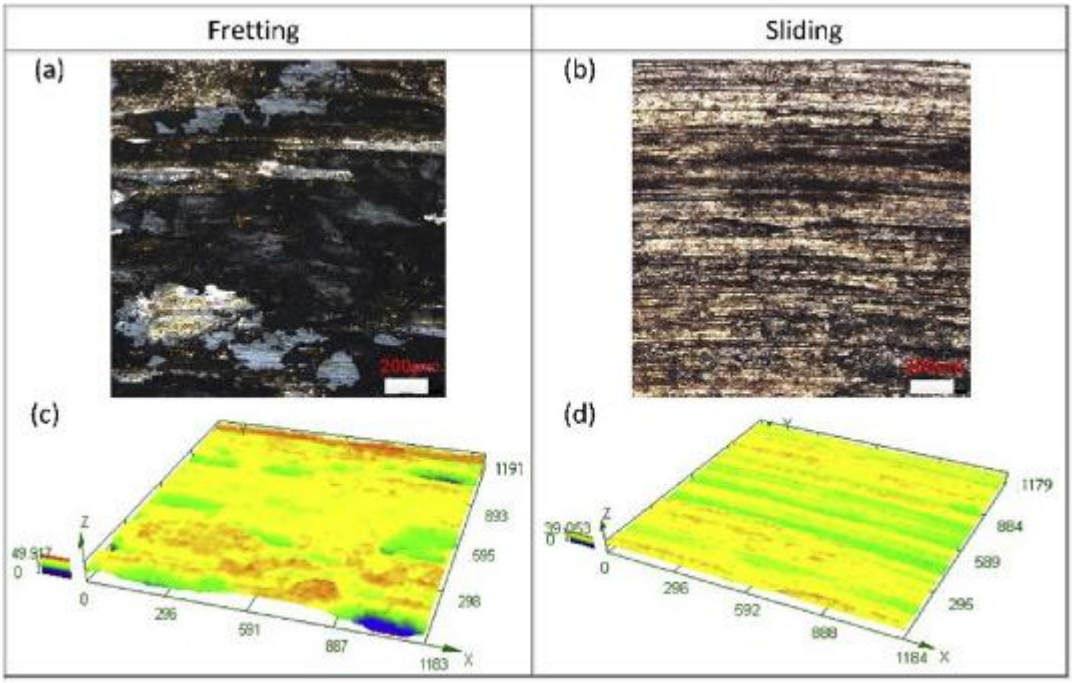

Fig. 9. Optical and 3D morphologies of the fretting and sliding wear traces: (P = 106N).

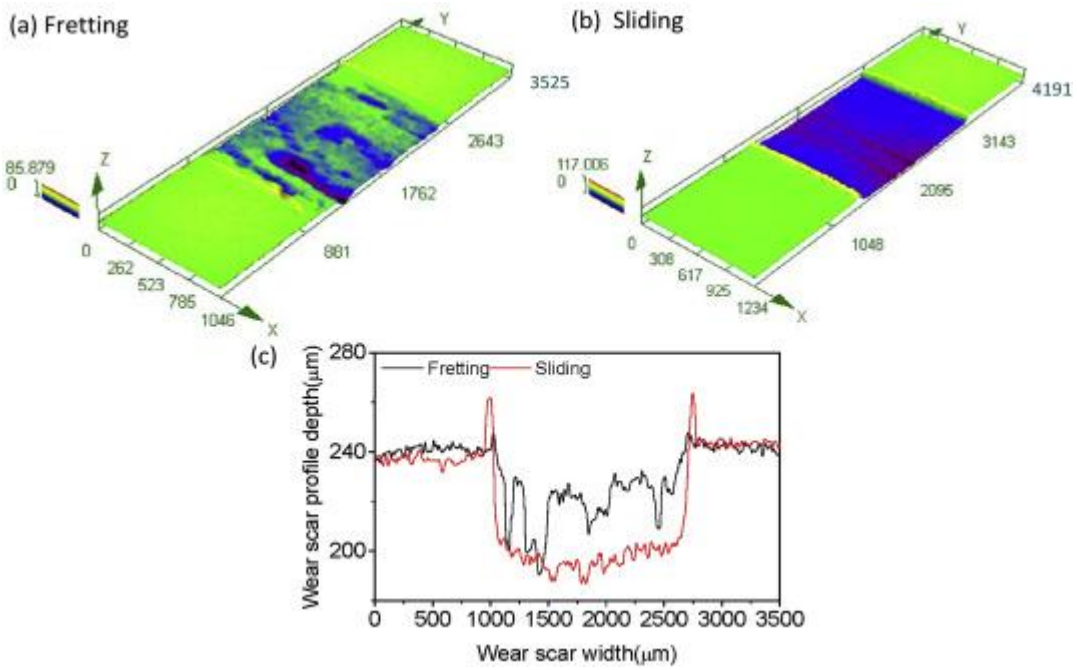

Fig. 10. Typical 3D and 2D cross-sectional profiles of the fretting and sliding wear traces: (P = 106N).

Typical SEM morphologies of the fretting and sliding wear traces are shown in Fig. 11 and Fig. 12, respectively. Under fretting condition, the wear process can lead to material removal (wear), nucleation and propagation of cracks (fatigue), and there is a competition between them [39]. From Fig. 11 it can be seen that the flake pits and cracks are observed on the fretting worn surfaces. The large flake pits are formed by the crack propagating during the relative movement. As plastic deformation accumulates, cracks are preferentially nucleated below the surface, but not at the surface, because a highly compressive stress exists just below the contact region. Once cracks are formed, further deformation will cause the cracks to extend and propagate parallel to the surface at a depth, and then connect to neighboring ones. Finally, the cracks shear to the surface, resulting in the delamination of large flake pits. Under sliding condition, as seen in Fig. 12, the worn surface is mainly characterized by numerous wide and deep grooves paralleled to the sliding direction, accompanied by serious plastic deformation. Besides, almost no cracks can be observed on the worn surfaces, indicating that the fatigue velocity was much lower than the wear velocity under the sliding condition.

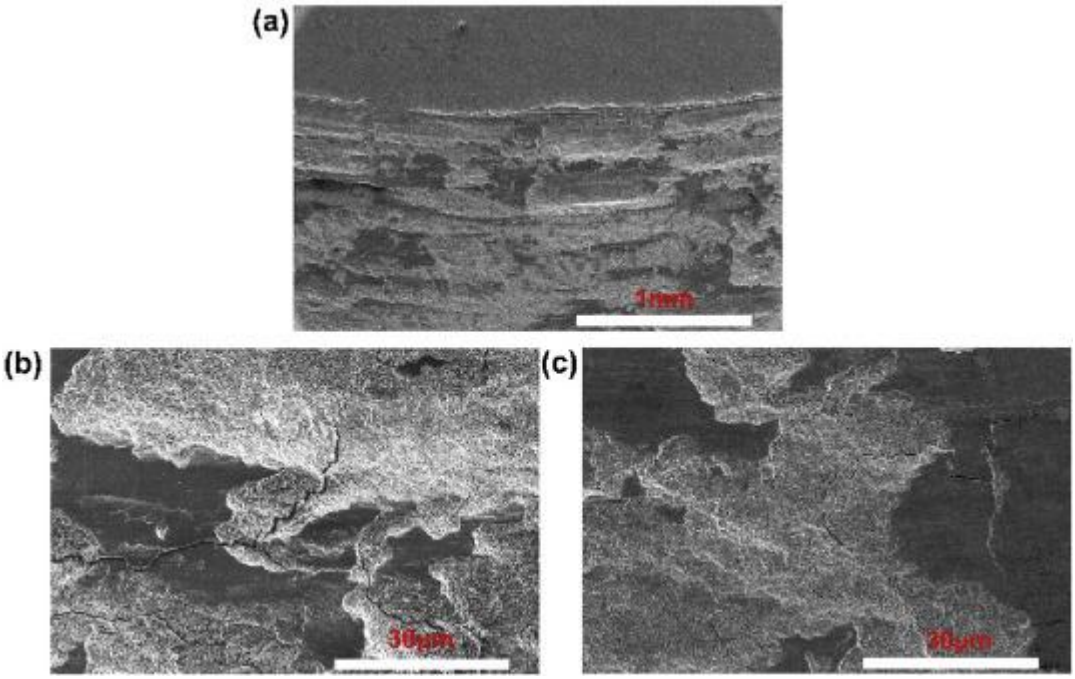

Fig. 11. SEM morphologies of the fretting worn surfaces: (P = 106N).

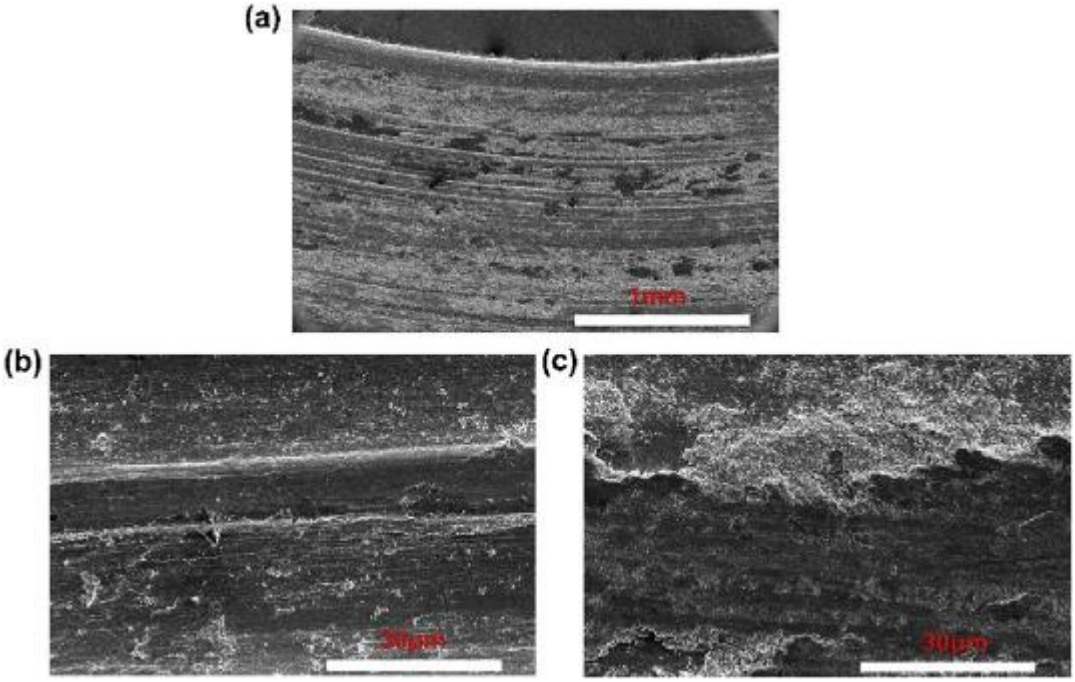

Fig. 12. SEM morphologies of the sliding worn surfaces: (P = 106N).

Fig. 13 displays the cross-sectional morphologies of the fretting and sliding wear traces. Fig. 13(a) shows a thick compacted debris bed and a thin flake-like sheet formed on the fretting specimen. Comparatively, the wear debris layer is much thinner and almost no cracks can be observed on the sliding morphology (Fig. 13(b)). The surface hardness of the region around the wear track has also been measured. Fig. 14 presents the micro hardness of the areas inside and outside of the fretting and sliding wear tracks. It can be seen that the wear track hardness is higher than that of the unworn surface, which may be attributed to the strain

hardening of the material during the wear process. Strain hardening of the worn surface may improve the wear resistance of the material, in terms of the adhesive theory given by Archard [40]. It is generally accepted that the wear loss is approximately inversely proportional to the hardness of the target material. It can also be seen that the hardness of the fretting wear track is much higher than the sliding wear track, indicating that the strain hardening of wear track was more serious under fretting than under sliding condition. Which is partly the reason why the fretting wear volume was smaller than the sliding wear volume.

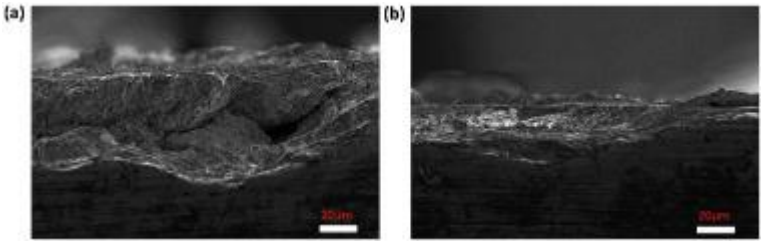

Fig. 13. Cross-sectional SEM images of the fretting and sliding wear traces.

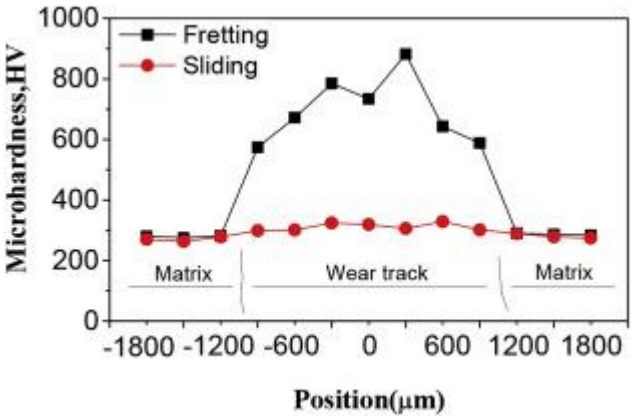

Fig. 14. Micro-hardness of CuNiAl specimen outside and inside wear traces.

3.4. Wear debris analysis

Wear debris of the fretting and sliding tests were collected and examined by the 3D optical microscope, as shown in Fig. 15. In fretting tests (Fig. 15(a)), the flake debris broke off and then grounded and crushed into fine particles. But due to the small amplitude, some of them were stuck in the contact interfaces and did not oxidize adequately, so they present the color of dark green. In sliding tests (Fig. 15(b)), some of the substrate material peeled off by the abrasion directly, so besides fine particles, the debris also contains large flakes, chips. But due to the large relative movement amplitude, the fine debris could contact with the air and oxidize adequately. So the fine debris presents the dark color. The large flakes, chips presented the brown color of CuNiAl by naked eye, but it could not be identified by the microscope due to reflection (Fig. 15(b)).

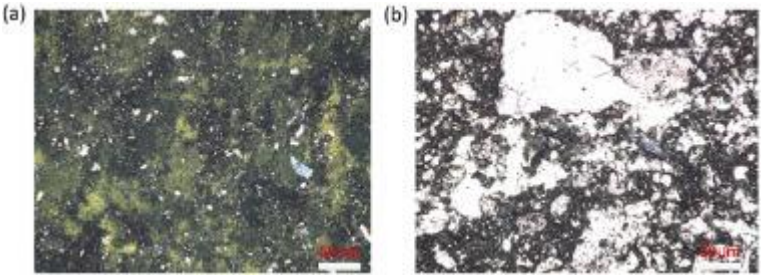

Fig. 15. Optical micrographs of wear debris: (a) Fretting test; (b) Sliding test.

In fretting tests, a thick debris bed was formed in the contact interface by the stuck fine particles. The appearance of debris bed may lead to the following factors: 1) It could attribute to the decrease of the real contact area by the participation of load-carrying; 2) Though the stuck fine debris could also cause abrasive wear, but it play a better role as solid lubricant to decrease the wear effectively [41]. While in sliding tests, the wear debris which contains large flakes, chips mainly played the role as abrasion to aggravate the abrasive wear. This is part of the reason why the fretting wear rate was much lower than the sliding wear rate.

The chemical composition of the wear debris was analyzed by XRF and is given in Fig. 16. It can be seen that compared with the base material of CuNiAl (Table 1), there was an obvious increase of Al and a decrease of Cu in the fretting debris, which can be explained that the Al element was easier to be oxidized than Cu, and the oxide Al2O3 was more brittle than CuO and easier to be fall off the base material and into the debris. Cu and Al were the main element components of the debris, so the increase of Al element also lead to the decrease of Cu element. Besides, compared with the CuNiAl, there was an increase of Cr and Mo in the fretting wear debris, indicating that a transfer of elements from the upper specimen to the lower specimen occurred. The element contents of the sliding wear debris were close to the base material of CuNiAl, which was because in the sliding tests, the wear rate was high, most of the wear debris was the material which directly removed from the substrate.

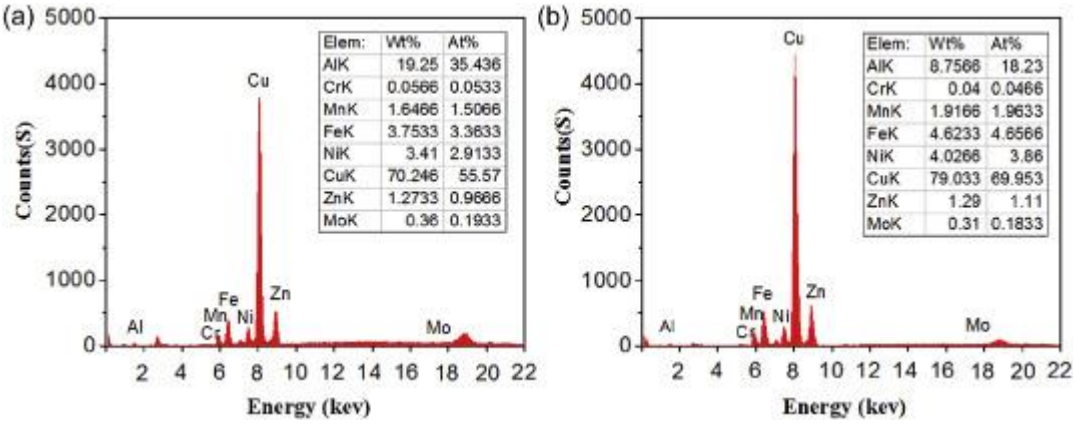

Fig. 16. XRF analysis of the wear debris: (a) Fretting test; (b) Sliding test.

4. Conclusion

Torsional fretting and torsional sliding wear behavior of CuNiAl against 42CrMo4 were comparatively investigated under dry condition with a flat on flat torsional tester. The following conclusions can be drawn from the present investigation:

(1)When the normal load increased, the fretting friction coefficient decreased slightly but the sliding friction coefficient decreased dramatically. Besides, the increase of normal load also lead to an obvious increase of wear volumes and accumulated dissipated energy. However no regular effects of angular speed on them were observed.

(2)In fretting tests, strain hardening of the wear trace track was more severe, besides, some debris were stuck in the contact interface and worked as solid lubricant, so the fretting wear rate was much lower than the sliding wear rate.

(3)The dominant wear mechanisms for the fretting tests were oxidation wear, cracks and delamination, while for the sliding tests were abrasive wear and plastic deformation.

Acknowledgements

This work was supported by the National Natural Science Foundation of China (Grant Nos. 51421062, 51575235), National Basic Research Program of China (2014CB046705).

References

[1]S. Wang, C. Niu, Torsional tribological behavior and torsional friction model of polytetrafluoroethylene against 1045 Steel PloS One, 11 (2016), p. e0147598

[2] H. Zhang, L. Blunt, X. Jiang, et al., The significance of the micropores at the stem–cement interface in total hip replacement, J Biomaterials Sci Polym Ed, 22 (2011), pp. 845–856

[3]M. Godjevac, Wear and friction in a controllable pitch propeller, Doctoral dissertation Delft University of Technology, TU Delft (2010)

[4]M. Martelli, M. Figari, M. Altosole, et al., Controllable pitch propeller actuating mechanism, modelling and simulation, Proc Institution Mech Eng Part M J Eng Marit Environ, 228 (2014), pp. 29–43

[5]H.Y. Zhang, L.A. Blunt, X.Q. Jiang, et al.,The influence of bone cement type on production of fretting wear on the femoral stem surface: a preliminary study, Clin Biomech, 27 (2012), pp. 666–672

[6]J.D. Lemm, A.R. Warmuth, S.R. Pearson, et al., The influence of surface hardness on the fretting wear of steel pairs—its role in debris retention in the contact, Tribol Int, 81 (2015), pp. 258–266

[7]Q. Wang, H. Wang, Y. Wang, et al., The influences of several carbon additions on the fretting wear behaviors of UHMWPE composites, Tribol Int, 93 (2016), pp. 390–398

[8]H. Quan, S. Gao, M. Zhu, et al., Comparison of the torsional fretting behavior of three porous titanium coatings for biomedical applications, Tribol Int, 92 (2015), pp. 29–37

[9] X. Zhang, H. Shen, J. Liu, et al., An efficient numerical model for predicting the torsional fretting wear considering real rough surface, Wear, 344 (2015), pp. 32–45

[10]Z.B. Xu, J.F. Peng, J.H. Liu, et al., Effect of contact pressure on torsional fretting fatigue damage of 316L austenitic stainless steel, Wear, 376 (2017), pp. 680–689

[11]S. Wang, S. Zhang, Y. Mao,Torsional wear behavior of MC nylon composites reinforced with GF: effect of angular displacement, Tribol Lett, 45 (2012), pp. 445–453

[12]S. Wang, B. Teng, S. Zhang, Torsional wear behavior of monomer casting nylon composites reinforced with GF: effect of content of glass fiber, Tribol Trans, 56 (2013), pp. 178–186

[13]K. Chen, D. Zhang, X. Yang, et al.,Research on torsional friction behavior and fluid load support of PVA/HA composite hydrogel, J Mech Behav Biomed Mater, 62 (2016), pp. 182–194

[14]J.F. Zheng, S. Yang, M.X. Shen, et al.,Study on rotational fretting wear under a ball-on-concave contact configuration,Wear, 271 (2011), pp. 1552–1562

[15]W. Lu, P. Zhang, X. Liu, et al.,Influence of surface topography on torsional fretting wear under flat-on-flat contact,Tribol Int, 109 (2017), pp. 367–372

[16]P. Zhang, W. Lu, X. Liu, et al.,Torsional fretting wear behavior of CuNiAl against 42CrMo4 under flat on flat contact,Wear, 380 (2017), pp. 6–14

[17]B.D. Leonard, F. Sadeghi, R.D. Evans, et al.,Fretting of WC/aC: H and Cr2N coatings under grease-lubricated and unlubricated conditions,Tribol Trans, 53 (2009), pp. 145–153

[18]M.A. Chowdhury, M.K. Khalil, D.M. Nuruzzaman, et al., The effect of sliding speed and normal load on friction and wear property of aluminum, Int J Mech Mechatron Eng, 11 (2011), pp. 53–57

[19] P. Zhang, W. Lu, X. Liu, et al., A comparative study on torsional fretting and torsional sliding wear of CuNiAl under different lubricated conditions, Tribol Int, 117 (2017), pp. 78–86

[20] K.J. Kubiak, T.G. Mathia, S. Fouvry, Interface roughness effect on friction map under fretting contact conditions, Tribol Int, 43 (2010), pp. 1500–1507

[21]L.A. Blunt, H. Zhang, S.M. Barrans, et al., What results in fretting wear on polished femoral stems, Tribol Int, 42 (2009), pp. 1605–1614

[22] W.S. Li, Z.P. Wang, L.U. Yang, et al., Corrosion and wear behaviors of Al-bronzes in 5.0% H2SO4 solution[J], Trans Nonferrous Metals Soc China, 19 (2) (2009), pp. 311–318

[23]R. Liu, D.Y. Li,Protective effect of yttrium additive in lubricants on corrosive wear

Wear, 225 (1999), pp. 968–974

[24]G. Cui, Q. Bi, S. Zhu, et al., Tribological behavior of Cu–6Sn–6Zn–3Pb under sea water, distilled water and dry-sliding conditions, Tribol Int, 55 (2012), pp. 126–134

[25] Q. Bi, W. Liu, J. Ma, et al., Tribocorrosion behavior of Ni-17.5 Si-29.3 Cr alloy in sulfuric acid solution, Tribol Int, 42 (2009), pp. 1081–1087

[26]B. Bhushan, W.E. Jahsman, Propagation of weak waves in elastic-plastic and elastic-viscoplastic solids with interfaces, Int J Solids Struct, 14 (1978), pp. 39–51

[27], B. Bhushan, Effect of shear strain rate and interface temperature on predictive friction models[C]//Westbury House,(1981)

[28], Y.S. Zhang, Z. Han, K. Lu, Fretting wear behavior of nanocrystalline surface layer of copper under dry condition, Wear, 265 (2008), pp. 396–401

[29]Y.S. Zhang, Z. Han,Fretting wear behavior of nanocrystalline surface layer of pure copper under oil lubrication, Tribol Lett, 27 (2007), pp. 53–59

[30]W. Huang, B. Hou, Y. Pang, et al.,Fretting wear behavior of AZ91D and AM60B magnesium alloys,Wear, 260 (2006), pp. 1173–1178

[31] H. Ding, Z. Dai, S.C. Skuiry, et al., Corrosion wear behaviors of micro-arc oxidation coating of Al 2 O 3 on 2024Al in different aqueous environments at fretting contact, Tribol Int, 43 (2010), pp. 868–875

[32]E. Sauger, S. Fouvry, L. Ponsonnet, et al.,Tribologically transformed structure in fretting

Wear, 245 (2000), pp. 39–52

[33]A. Ramalho, J.C. Miranda,The relationship between wear and dissipated energy in sliding systems, Wear, 260 (2006), pp. 361–367

[34]A. Ramalho, J.C. Miranda, Friction and wear of electroless NiP and NiP+ PTFE coatings

Wear, 259 (2005), pp. 828–834

[35]K. Jin, Z. Qiao, S. Zhu, et al.,Friction and wear properties and mechanism of bronze–Cr–Ag composites under dry-sliding conditions, Tribol Int, 96 (2016), pp. 132–140

[36]K.J. Kubiak, T.W. Liskiewicz, T.G. Mathia, Surface morphology in engineering applications: influence of roughness on sliding and wear in dry fretting, Tribol Int, 44 (2011), pp. 1427–1432

[37]S. Fouvry, P. Kapsa, L. Vincent, An elastic–plastic shakedown analysis of fretting wear

Wear, 247 (2001), pp. 41–54

[38]G. Srinath, R. Gnanamoorthy, Effect of nanoclay reinforcement on tensile and tribo behaviour of Nylon 6, J Mater Sci, 40 (2005), pp. 2897–2901

[39]P.H. Shipway, D.G. McCartney, T. Sudaprasert, Sliding wear behaviour of conventional and nanostructured HVOF sprayed WC–Co coatings, Wear, 259 (2005), pp. 820–827

[40]J.F. Archard, Contact and rubbing of flat surfaces, J Appl Phys, 24 (1953), pp. 981–988

[41] Z.B. Cai, M.H. Zhu, X.Z. Lin, Friction and wear of 7075 aluminum alloy induced by torsional fretting, Trans Nonferrous Metals Soc China, 20 (2010), pp. 371–376